Population-based cortical mapping of callosal connections in the human brain

Yirong Xiong
Beijing Normal University
Liyuan Yang
Beijing Normal University
Changtong Wang
Beijing Normal University
Chenxi Zhao
Beijing Normal University
Junhao Luo
Beijing Normal University
Di Wu
Beijing Normal University
Yiping Ouyang
The Queen's University of Belfast Joint College, China Medical University
Michel Thiebaut de Schotten
CNRS, University of Bordeaux https://orcid.org/0000-0002-0329-1814
Gaolang Gong (gaolang.gong@bnu.edu.cn)
Beijing Normal University https://orcid.org/0000-0001-5788-022X

Resource

Keywords: Corpus callosum, cerebral cortex, cortical topography, callosal connection, diffusion MRI

Posted Date: October 31st, 2022

DOI: https://doi.org/10.21203/rs.3.rs-2210117/v1

Additional Declarations: There is **NO** Competing Interest.

Population-based cortical mapping of callosal connections in the human brain

Yirong Xiong[1], Liyuan Yang[1], Changtong Wang[1], Chenxi Zhao[1], Junhao Luo[1], Di Wu[1], Yiping Ouyang[2], Michel Thiebaut de Schotten[3, 4], Gaolang Gong[1, 5, 6*]

[1] State Key Laboratory of Cognitive Neuroscience and Learning & IDG/McGovern Institute for Brain Research, Beijing Normal University, Beijing, China

[2] The Queen's University of Belfast Joint College, China Medical University, Shenyang, China

[3] Brain Connectivity and Behaviour Laboratory, Sorbonne Université, Paris, France

[4] Groupe d'Imagerie Neurofonctionnelle, Institut des Maladies Neurodégénératives-UMR 5293, Centre National de la Recherche Scientifique, Commissariat à l'Energie Atomique, University of Bordeaux, Bordeaux, France

[5] Beijing Key Laboratory of Brain Imaging and Connectomics, Beijing Normal University, Beijing, China

[6] Chinese Institute for Brain Research, Beijing, China

Running title: Cortical mapping of callosal connections

*** Correspondence:**

Dr. Gaolang Gong
National Key Laboratory of Cognitive Neuroscience and Learning & IDG/McGovern Institute for Brain Research, Beijing Normal University,
#19 Xinjiekouwai Street, Beijing 100875, China
Tel: +86 10 58804678; Fax: +86 10 58804678
E-mail: gaolang.gong@bnu.edu.cn

Abstract

The corpus callosum (CC) is the principal white matter (WM) bundle supporting communication between the two brain hemispheres. Despite its importance, a comprehensive mapping of callosal connections is still lacking. Here, we constructed the first bidirectional population-based callosal connectional atlas between the midsagittal section of the CC and the cerebral cortex of the human brain by means of diffusion-weighted imaging tractography. The estimated connectional topographic maps within this atlas have the most fine-grained spatial resolution, demonstrate histological validity, and were reproducible in two independent samples. This new resource will revolutionize the investigation of interhemispheric communication and come with a user-friendly companion online tool (*CCmapping*) for easy access and visualization of the atlas.

Key words: Corpus callosum, cerebral cortex, cortical topography, callosal connection, diffusion MRI

Introduction

The corpus callosum (CC) is the major white matter (WM), integrating information and coordinating cognitive processing between the two cerebral hemispheres[1–5]. The midsagittal section of the corpus callosum (mCC) is usually preferred to measure this prominent fiber bundle in postmortem brain samples or *in vivo* magnetic resonance images for simplicity, as it summarizes the properties of all callosal fibers. Various mCC measures (e.g., morphology and diffusivity parameters) have shown significant correlations with biological factors (e.g., age and sex), cognitions, and brain diseases[6–9].

Mapping detailed connections between the mCC and cortical regions is fundamental for investigating and understanding interhemispheric communication. Knowing what mCC regions are connected to is critical to understanding their functions. This mapping can be achieved for animals by chemical tracing methods[10–16], but these methods are not feasible for the human brain due to their invasive nature. Instead, correlating focal cortical lesions with Wallerian degeneration in the mCC was applied to achieve such mapping. However, this type of *in vitro* method is not comprehensive and requires postmortem lesioned-brain[17].

More recently, diffusion MRI techniques have been used noninvasively to map human CC connections *in vivo*. Specifically, the callosal fibers passing through the mCC were virtually reconstructed as streamlines using diffusion MRI tractography. In so doing, mCC voxels were directly associated with cortical regions[18–20]. Such approaches are more commendable than others, such as the geometrical parcellation of the mCC[21] only have an approximate relationship with cortical regions. A few studies also applied this approach to obtain topographic maps of the mCC for particular cortical regions that were defined anatomically[22–24] or functionally[25–27]. These studies proved the feasibility of diffusion MRI tractography-based mapping for human brain callosal connections. They are, however, limited by only partial topographic mapping, old-fashioned diffusion MRI acquisition and tractography algorithms, and a very small number of scanned subjects. To date, a complete callosal atlas containing high-quality bidirectional topographic maps between the mCC and its connected cortical regions is lacking. This substantially impedes sophisticated investigations of callosal connections and cortical communication between the two hemispheres of the human brain.

The present study constructed a comprehensive population-based human brain callosal atlas containing detailed connectional topographies between mCC voxels and cortical regions. The notably high-quality diffusion MRI datasets from the ~1000 Human Connectome Project (HCP) healthy young adults[28], together with well-refined diffusion MRI tractography, were used to virtually reconstruct callosal fibers (Fig. 1). For each mCC voxel, two weighted cortical connectional topographic maps were generated at the population level; for each pair of homotopic cortical regions, two weighted mCC connectional topographic maps were generated at the population level. Furthermore, we developed an online tool to 1) interactively visualize such a comprehensive atlas and 2) estimate cortical or mCC topographic maps for customized mCC or cortical regions of interest (ROIs).

Results

Cortical topographic maps for mCC voxels and subdivisions

For each voxel (1554 in total) or each subdivision on the template mCC, two population-based cortical topographic maps were generated: the populational probability (PP) weighted and relative streamline number (RSN) weighted maps on the *32k_fs_LR* surface.

For each cortical topographic map, a cutoff value for the PP or RSN weights was estimated at the statistical significance level of p = 0.05. In Fig. 2A, we show both nonthresholded and thresholded PP-weighted topographic maps for 10 selected voxels that are approximately evenly distributed across the template mCC. In addition, Fig. 2B-2D shows the PP-weighted topographic maps for each mCC subdivision from the well-known Aboitiz[29], Witelson[21], and Hofer parcellation[19]. The RSN-weighted topographic maps for these selected mCC voxels or subdivisions are illustrated in Fig. S1, and their spatial patterns are similar to the PP-weighted ones. The topographic maps for all mCC voxels and subdivisions can be easily viewed and accessed via the *CCmapping* (www.ccmapping.org) below.

As shown, the estimated cortical topographic maps are highly compatible with prior information in neuroanatomy. The voxels and subdivisions in the most anterior mCC part (e.g., genu) mainly contain callosal streamlines projecting to the prefrontal cortex. The anterior and middle parts of the mCC mainly contain callosal streamlines projecting to the premotor and supplementary motor areas. The most posterior part of the mCC contains callosal streamlines projecting to the parietal, temporal, and occipital cortices.

mCC topographic maps for homotopic cortical regional pairs

To estimate mCC topographic maps for homotopic cortical regional pairs, the entire cortical surface was parcellated at three different spatial resolutions: Brainnetome atlas (BNA, 105 pairs of homotopic cortical regions)[30], HCP multimodal parcellation (HCPMMP, 180 pairs of homotopic cortical regions)[31], and mirrored 1000-Parcels version of the Schaefer2018 Parcellation (Schaefer_L/Schaefer_R, 500/498 pairs of homotopic cortical regions)[32].

For each homotopic regional pair, PP-weighted and RSN-weighted mCC topographic maps were generated. For each mCC topographic map, a cutoff value for the PP or RSN weights was also estimated at the statistical significance level of p = 0.05. For each parcellation scheme, we randomly selected six pairs of homotopic regions that were approximately evenly distributed across the frontal, parietal, temporal, and occipital cortices. Both nonthresholded and thresholded PP-weighted and RSN-weighted topographic maps were illustrated for the six pairs of homotopic regions (Fig. 3 and Fig. S2). Again, the topographic maps for all pairs of homotopic regions can be easily viewed, and accessed via the *CCmapping*.

In concordance with prior information in neuroanatomy, callosal streamlines connecting bilateral prefrontal cortices mainly pass through the very anterior part of the mCC. Callosal streamlines connecting the bilateral premotor and motor cortices mainly pass through the anterior and middle parts of the mCC. Callosal streamlines connecting the bilateral parietal, temporal, and occipital cortices mainly pass through the posterior parts of the mCC.

Validity and reproducibility

To evaluate the validity of our estimated topographic maps, we summarized the histological results of mapping the monkey or human brain between the mCC and cortical regions in the literature (Table 1). Specifically, we used the *CCmapping* to locate the most matched HCPMMP region or mCC subdivision for the injection site of the chemical tracer in each relevant study (8 in total). We then extracted the topographic maps from our atlas. As shown in Fig. S3:1-8, the comparison showed that our estimated topographies are highly consistent with previously reported histological data.

We evaluated the reproducibility of the estimated topographic maps for each mCC voxel or homotopic cortical regional pair by comparing the re-estimated topographic maps from two split-half HCP samples using Pearson correlation and intraclass correlation (ICC). As illustrated in Fig. 4 and Fig. S4, both Pearson correlation and ICC values are quite high (almost close to 1) for most mCC voxels. This indicates a high similarity of the cortical PP-weighted or RSN-weighted maps between the two split-half samples, suggesting a limited sampling effect on the results. Regarding the mCC topographic maps, most homotopic regional pairs showed high Pearson correlation and ICC values (almost close to 1). This demonstrates a high similarity of the resultant mCC PP-weighted or RSN-weighted maps between the two split-half samples. A few insular and temporal regions, however, showed medium and even low Pearson correlation and ICC values. Overall, the Schaefer_L/Schaefer_R parcellation has a lower Pearson correlation and ICC than the BNA and HCPMMP, suggesting a lower reproducibility of mCC topographic maps for higher spatial resolution of cortical parcellation.

To evaluate potential genetic confounding effects on our results, we compared the topographic maps from the 93 unrelated HCP subjects with the main maps from the total HCP subjects. As shown in Fig. 4 and Fig. S4, most Pearson correlations and ICCs are quite high. This indicates a high similarity of PP-weighted and RSN-weighted topographic maps between the unrelated and total HCP samples, indicating a limited sibling effect on our results.

Finally, the key algorithm parameter, i.e., the initially generated callosal streamlines of our tractography, showed minimal effect on our results. As illustrated in Fig. 5 and Fig. 5S, the resultant PP-weighted and RSN-weighted topographic maps estimated from more initially generated callosal streamlines have high similarity with our main results (i.e., from 10 M initially generated callosal streamlines). This indicates that the 10 M initially generated callosal streamlines in our main analysis reached a stable estimation for these connectional topographic maps at the population level.

CCmapping

We developed an online tool, i.e., *CCmapping* (www.ccmapping.org), to interactively visualize and export our generated mCC or cortical topographic maps. Fig. 6A illustrates the main interface for this tool. The left side of the interface, i.e., the mCC panel, supports 1) voxel or subdivision selection on the mCC while viewing cortical topographic maps and 2) visualization of mCC topographic maps after selecting a specific cortical region within the cortical surface panel on the right side. The right side of the interface, i.e., the cortical surface panel, supports 1) region selection on the cortical surface while viewing mCC topographic maps and 2)

visualization of cortical topographic maps after selecting a specific mCC voxel or subdivision within the mCC panel on the left side. The tool provides a set of statistics of the involved callosal streamlines (e.g., mean length, number, and connected cortical functions) in an embedded information box.

All our estimated cortical or mCC topographic maps above are openly accessible through *CCmapping*. By default, after loading the requested mCC or cortical topographic map, *CCmapping* displays the thresholded map at $p = 0.05$. The cutoff value can be freely adjusted using the thresholding bar. Fig. 6B-C illustrates two example snapshots of visualizing mCC and cortical topographic maps.

Moreover, *CCmapping* also provides file-uploading services, which enable online estimation and visualization of topographic maps for a customized region of interest (ROI) on the mCC or cortical ROI. The customized ROI mask file could be uploaded to the upper right corner within the mCC or cortical surface panel. Fig. 6D-E illustrates mCC and cortical topographic maps for two example customized cortical or mCC ROIs.

Application of resultant topographic maps

To confirm whether positional dependence exists between the callosal axon and its connected cortical regions, we separately evaluated the correlation of the Y coordinates (i.e., the anterior-posterior direction) and Z coordinates (i.e., the dorsal-ventral direction) of mCC voxels with the barycenter of their connected cortical regions. Fig. 7A confirms that there is a significant correlation in both directions (Y coordinate: $r = 0.99$, $p < 0.0001$; Z coordinate: $r = 0.96$, $p < 0.0001$). These correlations indicate that 1) the callosal fibers passing through the anterior part of the mCC are more likely to connect the anterior cortical region and 2) the callosal fibers passing through the dorsal part of the mCC are more likely to connect the dorsal cortical region.

Next, to test whether the myelin content of parcellated cortical regions relates to the composition of their connected callosal fibers, we evaluated the correlation of the T1/T2 ratio values of cortical regions with the neurite density index (NDI) and orientation dispersion index (ODI) values of their passing mCC region[33]. For all 4 cortical parcellations, significant negative correlations (all $ps < 0.05$) were observed for both NDI and ODI (Fig. 7B). Accordingly, more cortical myelin content is associated with less fiber density and orientational dispersion on the mCC. This result suggests a biological association between cortical myeloarchitecture and cortical information transfer to the other hemisphere.

Discussion

Using a high-quality diffusion MRI dataset from a large group of healthy adults we constructed the first bidirectional population-based connectional atlas between the mCC and cerebral cortex of the human brain. This comprehensive atlas provides connectional topographic maps for both the mCC and cortical surface at the highest resolution ever (i.e., mCC voxel and small cortical patch). The validity and reproducibility of the estimated topographic maps were proven by comparisons with existing histological data and between population sampling, respectively. A user-friendly interactive online tool, i.e., *CCmapping*, was further developed for easily visualizing and accessing these maps. Through these topographic maps, preliminary analyses

revealed positional dependence and microstructural correlations between callosal fibers and their connected cortical regions in the human brain, demonstrating the added value of these maps in understanding human callosal connections.

There are hundreds of reports showing significant group differences in regions of the mCC[8,34,36]. For each reported cluster or region on the mCC, it is always necessary to interpret its functional relevance. To achieve this, previous studies typically chose to map the observed mCC clusters or regions onto the mCC subdivisions of the Witelson or Hofer parcellation and accordingly inferred their connected cortical regions in terms of the corresponding subdivision (e.g., genu, body, and splenium), since the cortical connectional topographies have been summarized to some degree for each of the subdivisions[19,21]. However, this approach suffers from two flaws: 1) for each mCC subdivision, the summarized connectional topographies are qualitative in nature and lack a well-defined boundary on the cortical surface; 2) clusters or regions of different sizes and locations on the same subdivision of the mCC would end up with similar inferred connectional topographies, which is obviously problematic. For any predefined or observed cluster or region on the mCC that does not exactly match one entire subdivision, there have been no (even coarsely) summarized cortical connectional topographies available. These issues can be well addressed by our currently constructed callosal atlas, which offers pre-estimated cortical topographic maps at the mCC voxel level and is able to provide quantitative cortical topographies for any cluster or region on the mCC. Particularly, offering specific cortical maps for clusters or regions on the mCC enables quantitative in-house analyses between mCC and cortical measures with the investigators' multimodal data, apart from simply inferring the function of the mCC cluster through its connected cortical regions.

Mapping topographies on the mCC for callosal fibers connecting different cortical regions helps understanding within-CC topographic organization. The mCC topographies for cortical regions have been applied to parcellate the entire mCC into subdivisions[18–20]. To measure callosal fibers underlying visual and motor processing between the two hemispheres, previous studies have mapped the mCC topographies for the visual and motor areas[25–27]. Moreover, a few studies have elegantly mapped the mCC topographies for all parcellated cortical regions from the entire cerebral cortex[22–24]. The resultant mCC topographies in these studies, however, are limited by the low resolution of their cortical parcellations, i.e., too large a size for each cortical region (the maximum total number of cortical regions being less than 50). In contrast to these studies, our currently constructed callosal atlas offers detailed mCC topographies for cortical parcellations at much higher resolution, i.e., 105 BNA-based cortical regions, 180 HCPMMP-based cortical regions, 500 Schaefer_L-based cortical regions, and 498 Schaefer_R-based cortical regions, improving the applicability of mCC topographic maps. Such advanced CC mapping will permit quantitative in-house analyses between mCC and cortical measures with more precision and flexibility.

The estimated topographic maps are consistent with existing histological data in the literature (i.e., the gold standard available). Such validity likely relates to our state-of-the-art diffusion MRI acquisition and tractography, as well as the population-based nature of these maps. To minimize classical tractography errors, high-angular resolution diffusion MRI data, cutting-edge local orientation modeling, sophisticated tractography algorithms, and post fiber filtering

were employed[37–39]. Additionally, the ultimate topographic maps were generated by combining individual tractography data from almost 1000 healthy adults. The combination across such a large group of healthy adults can effectively reduce noises or errors that occur randomly at the individual level, further improving the accuracy of the ultimate topographic maps.

The present study offers efficient solutions for two key issues of usability: 1) thresholding and 2) accessing these maps. First, rigorously thresholding a brain map is often required before analyses and interpretation. Numerous thresholding methods have been developed for statistical parametric maps (e.g., t map, p map)[40–42]. However, they are not suitable for our data. Therefore, an in-house thresholding method based on permutation and Moran spectral randomization was developed[43], which should be usable for other studies with similar data structures. Using this method, a threshold value at the statistical significance level of $p = 0.05$ was estimated and saved for each mCC or cortical topographic map. Through the statistically meaningful topographic boundary or mask on the thresholded maps, the topography-based analysis and interpretation are greatly facilitated. Second, viewing and accessing the estimated topographic maps is also challenging, as the entire atlas includes thousands of cortical or mCC topographic maps, each linking to a selected mCC voxel/subdivision or cortical region. Given the complex data correspondence, simultaneously showing the selected mCC voxel/subdivision or cortical region as well as its linked topographic map is essential for efficient viewing. Our solution for this is *CCmapping*, an online tool that was exclusively developed for visualizing and exporting the estimated topographic maps. Particularly, the *CCmapping* has prestored the estimated threshold values for all maps and the enormous amount of map files on the cloud. This allows for an interactive view of requested topographic maps in a modern web browser after quickly loading them from the cloud, a useful function for both research and educational purposes. Moreover, *CCmapping* supports exporting the loaded topographic maps to local files, enabling in-house analyses with specific topographic maps. Taken together, the two solutions above effectively boost the usability and accessibility of our atlas.

Previous studies have shown dorsal-ventral positional dependence for the specific local part of the CC[26,44]. Our findings replicated this positional dependence and extended this organizational principle to the entire human CC. Such organization minimizes the overall callosal fiber length, therefore supporting the optimal wiring hypothesis for the brain organization[45–47]. Additionally, this positional dependence is compatible with the notion that neuronal axons within each WM tract are positioned in an orderly manner in terms of their origination[44,48]. Moreover, this atlas revealed an association of callosal fiber microstructures with their connected cortical regions. Such an association further confirms a biological link between cortical myeloarchitecture and its information transfer to the other hemisphere[49]: sensorimotor cortices contain more myelin and communicate with the contralateral hemisphere by callosal fibers with larger diameters; association cortices contain less myelin and communicate with the contralateral hemisphere by callosal fibers with smaller diameters. Future investigation is warranted to determine the functional mechanisms underlying this link.

Finally, a few limitations should be addressed. First, the validation for our topographic maps is based on the histological data in the literature. These data are limited and describe relatively coarse anatomical locations, leading to our validation analysis at a very low resolution. Next,

our estimated maps are derived from healthy adults. It is unclear whether they can be extrapolated to other populations (e.g., newborns and patients with brain diseases). Future studies are encouraged to map topographic maps for other populations and even other species (e.g., macaque). Finally, in addition to the population-based atlas, individualized topographic maps are of great value for personalized analysis and interpretation but are beyond the scope of our current study. In future studies, the currently generated atlas can be taken as an initial point for accurately estimating the callosal connectional topographies at the individual level.

Materials and Methods

MRI dataset

The dataset included all possible HCP participants for whom both diffusion and T1 images were available. It comprised 928 healthy young adults (female/male: 503/425; age range: 22-37 years). Informed consent was obtained from all subjects, and the protocol was approved by the Institutional Review Board of Washington University. MRI scanning was performed using a customized Siemens Connectome Skyra 3T scanner. Diffusion-weighted (DW) images were acquired using a spin–echo echo-planar imaging (EPI) sequence with the following parameters: repetition time (TR) = 5520 ms, echo time (TE) = 89.5 ms, flip angle = 78°, FOV = 210 × 180 mm^2, matrix = 168 × 144, slices = 111, and resolution = 1.25 mm × 1.25 mm × 1.25 mm. Diffusion weightings of b = 0, 1000, 2000, and 3000 s/mm^2 were applied in the 18, 90, 90 and 90 directions, respectively. High-resolution 3D T1-weighted (T1W) images were acquired using a magnetization prepared rapid gradient echo (MPRAGE) sequence using the following parameters: TR = 2400 ms, TE = 2.14 ms, TI = 1000 ms, flip angle = 8°, FOV = 224 × 224 mm^2, and resolution = 0.7 mm × 0.7 mm × 0.7 mm. DW and T1W images were preprocessed using the HCP minimal preprocessing pipeline[50].

Individual midsagittal CC (mCC) and its alignment to the template

The HCP minimal preprocessing pipeline aligned the anterior commissure (AC), the AC–posterior commissure (PC) line, and the interhemispheric plane of the T1W images to the MNI template using a rigid transform of 6 degrees of freedom. This transformation maintains the original size and shape of the brain. On the resultant T1W image of each individual, the midsagittal plane slice was selected, and the mCC boundary was then manually outlined by a trained rater (D.W.). The mCC boundary of 50 randomly selected participants was outlined two weeks later by the rater to assess the manual outlining reliability. The Dice coefficient of the mCC masks ranged from 0.95 to 0.99 (mean: 0.98, SD: 0.009), and the intraclass correlation coefficient (ICC) of the mCC area reached 0.99.

To ensure voxel-wise comparability across individuals, the individual mCC was nonlinearly aligned to a manually outlined template mCC on the MNI152 template image[49]. Specifically, the 2D sagittal image of the template mCC was set as the target image (or the fixed image), and the 2D sagittal image of the individual mCC was set as the source image (or the moving image). The two 2D images were first smoothed with a 2D Gaussian smoothing kernel (sigma = 1) by using the 'imGaussfilt' function in MATLAB. Next, we linearly aligned the source image to the target image (i.e., performed a 2D affine transform of 8 degrees of freedom, including

translation, rotation, scaling, and shearing) using the 'imregtform' function in MATLAB. Next, we performed nonlinear registration from the linearly aligned source image to the target image using the demons algorithm that was implemented by the 'imregdemons' function in MATLAB. Here, three multiresolution image pyramid levels were used, and 100 iterations were estimated at each pyramid level. Gaussian smoothing (sigma = 1) was applied to regularize the accumulated displacement field at each iteration. To maximize the aligning accuracy, this whole nonlinear registration procedure was iterated 5 times. Finally, the linear and nonlinear displacement fields were merged, and this merged field can be used to transform the individual mCC into the template space. For each individual, the mCC alignment was carefully checked by visual inspection.

Callosal fiber tracking with diffusion MRI-based tractography

For each subject, diffusion MRI-based tractography was used to extract callosal fiber streamlines that passed through the individual mCC above. Specifically, fiber orientation distributions (FODs) of each voxel were first estimated using multi-shell, multi-tissue constrained spherical deconvolution with a harmonic order of 8 and default parameters using Mrtrix3[37,51]. Probabilistic fiber tracking was then performed using the 2nd-order integration over FODs (iFOD2) algorithm in Mrtrix3[52]. Given our focus on the callosal fibers, the mCC was set as an inclusion mask (i.e., saving only fibers traversing the mCC) in fiber tracking. Due to the ambiguous existence of callosal fibers connecting bilateral subcortical nuclei, all subcortical nuclei were set as exclusion masks (i.e., fibers traversing them were discarded). Here, subcortical nuclei, including the thalamus, hippocampus, amygdala, caudate, putamen, palladium, and accumbens, were extracted using the FIRST tool of the FMRIB Software Library (FSL)[53]. To improve the biological accuracy of the tractograms, the anatomically constrained tractography (ACT) framework was used, which incorporates prior anatomical information into the tractography[38]. The anatomical information was obtained by segmenting T1W images into tissue partial volume maps (PVMs) for WM, GM, and cerebrospinal fluid (CSF) using FSL tools. The resultant PVM images were then taken as anatomical priors into the ACT framework. For each HCP participant, the minimal preprocessed T1W image was well aligned with the DW images; therefore, the mCC and PVM images were already in the DW image space. The detailed fiber-tracking parameters were as follows: step size = 0.625 mm (default), maximum curvature per step = 45°, FOD threshold = 0.05, and length range = 2.5-250 mm. For each subject, 10 million streamlines were generated by seeding from and ending into the ACT-generated GM-WM interface (GMWMI).

Mapping cortical topography for mCC voxels

For each streamline, the passing coordinate was first estimated on the individual mCC and then transformed onto the template mCC of the MNI space using the spatial alignment of the mCC above. All passing streamlines therefore could be determined for each voxel or a cluster of voxels on the template mCC.

For each HCP subject, the minimal preprocessing pipeline provides FreeSurfer-generated individual pial and white surfaces resampled onto the standard *32k_fs_LR* mesh (containing ~32k vertices for each hemispheric surface). For each streamline, its connected cortical vertex

was determined as the closest vertex on the white surface within a sphere with a 2-mm radius centered at its endpoint (one in each hemisphere). We excluded the streamlines that failed to find any vertex within a sphere within a 2-mm radius centered at its endpoint.

For each voxel of the template mCC (1554 voxels in total), a cortical *32k_fs_LR* surface map of streamline count (i.e., connectional topography) was then derived for each subject using all passing streamlines. At the group level, we adopted two weighting schemes for such connectional topographic maps: populational probability (PP) and relative streamline number (RSN). For the PP-weighted topographic map, we first binarized the individual maps of streamline count and later calculated a probability map across all individuals. For the RSN-weighted topographic map, we normalized the individual maps of streamline count by scaling the total number of all included callosal streamlines of each subject to 5 million and then averaged them.

In addition, we applied the same strategies discussed above to estimate cortical connectional topographies for mCC subparts that were derived from three influential parcellations of mCC: the Witelson (6 mCC subdivisions)[21], Aboitiz (10 mCC subdivisions)[29], and Hofer (5 mCC subdivisions) parcellations[19].

Mapping mCC topography for cortical regions

It is unnecessary and computationally impractical to map the mCC topography for cortical regions at the vertex level. Here, we applied several widely used atlases to parcellate the entire cortical surface into cortical regions at different spatial resolutions: ~100 regions, ~200 regions, and ~500 regions within each hemisphere. The first is the Brainnetome atlas (BNA), which was derived from WM connectional information[30]. It includes 105 cerebral cortical regions in each hemisphere. The second is HCP multimodal parcellation (HCPMMP), which is based on multiple neurobiological properties[31]. It includes 180 cerebral cortical regions in each hemisphere. In these two parcellation schemes, cortical regions are homotopically paired between the two hemispheres. The other two parcellations are from the 1000-Parcels version of the Schaefer2018 Parcellation that was based on resting-state functional connectional information[32]. It includes 500 and 498 cerebral cortical regions in the left and right hemispheres, respectively, and these regions are not homotopic between the two hemispheres. We therefore mirrored the parcellation of each hemisphere to the opposite hemisphere, resulting in two symmetric parcellations: Schaefer_L and Schaefer_R.

For each pair of homotopic cortical regions, all connected streamlines and their passing voxels on the template mCC can be determined. Accordingly, a streamline count map of template mCC (i.e., connectional topography) was derived for each subject. At the population level, we also generated two topographic maps, the PP-weighted and RSN-weighted maps, for each pair of homotopic cortical regions.

Reproducibility analysis

To test the sampling effect on our currently observed population-based topographic maps, we re-estimated topographic maps with split-half HCP samples (464 HCP subjects for each sample) and assessed the similarities of resultant topographic maps between the two split-half samples.

Next, to evaluate the sibling confounding effects on the maps, we re-estimated the topographic maps using the 93 unrelated (nonsibling) subjects from the HCP unrelated set and evaluated their similarities with the main maps. Finally, a larger number of initially generated callosal streamlines from tractography is preferred for estimating stable topographic maps. However, an excessively large number comes with a very large burden of data storage and computation. To assess whether the 10 M initially generated callosal streamlines from tractography for our main analysis was enough, we compared the topographic maps between our main scheme (i.e., 10 M streamlines) and validation schemes (i.e., from 13 M to 22 M streamlines) using the unrelated HCP subjects. For either cortical topographic maps or mCC topographic maps, both the Pearson correlation coefficient (r) and intraclass correlation coefficient (ICC) were used to quantify the degree of similarities between the two topographic maps.

Thresholding topographic maps

To determine a practically meaningful boundary for each population-based topographic map, we applied a permutation procedure and estimated a cutoff value at the statistically significant level of $p = 0.05$. Here, we take the population-based cortical topographic map for a mCC voxel/subpart as an example. For each subject, we first permuted the values on the individual-based topographic map by adopting Moran spectral randomization, which preserves the spatial autocorrelation of the map[43]. Using the resultant permutated individual-based maps, we then generated a randomized population-based topographic map with different resolutions and different weighting schemes, as described above. We repeated the same procedure 10000 times, resulting in 10000 randomized population-based topographic maps. The 95th percentiles of maximal values in the 10000 randomized population-based maps were calculated as the cutoff value, which corresponds to the statistical significance level $p = 0.05$ for weight values within the topographic map. Likewise, for each homotopic cortical regional pair, the cutoff value for its population-based topographic mCC map was estimated using the same permutation procedure.

An online interactive viewer for both mCC and cortical topographic maps

We developed a web-based viewer using JavaScript to interactively visualize each population-based topographic map above. This tool was largely based on the open-source library BrainBrowser[54]. BrainBrowser supports real-time visualization of the 3D cortical surface, brain volume, and various kinds of neuroimaging data in any modern web browser by WebGL, HTML5, and other technologies. In addition, Echarts and Node.js technologies were applied.

Application of mCC and cortical topographic maps

High-resolution connectional topographic maps are essential for CC studies, particularly those concerning the relationship between callosal fibers and connected cortical regions. As examples, we applied the estimated topographic maps above to perform two specific investigations as follows.

1) Neural axons within the WM tract are segregated in an orderly manner according to their originating topographies[48]. In line with this hypothesis, callosal axons originating from one dorsal region (i.e., M1) and another ventral region (i.e., S1) in mice showed strictly dependent

dorsal and ventral positioning on the midline[44]. However, it remains unclear whether such observed positional dependence can be generalized to the entire CC of the human brain. To answer this question, we conducted analyses as discussed further. For each voxel on the template mCC, we extracted its coordinate along the Z and Y axes. We extracted the barycenter coordinates of the connected cortical region of each voxel (derived from the thresholded cortical topographic map at $p = 0.05$) along the Z and Y axes. Here, the Z and Y coordinates represent relative positioning along the dorsal-ventral (D-V) and anterior-posterior (A-P) axes within the human brain, respectively. Pearson correlation between the two Z or Y coordinates was then evaluated across all mCC voxels. A significant Z or Y coordinate correlation indicates a D-V or A-P positional dependence between the callosal axon and the connected cortical regions across the entire CC.

2) Cortical myelin content and callosal fiber composition exhibit significant variation across the entire cortex and mCC, respectively. Recent studies found that cortical myelin content was correlated with callosal fiber length scaling. This suggests a biological link between cortical myeloarchitecture and the efficacy of cortical communication to the contralateral hemisphere[49]. To further determine whether the myelin content of parcellated cortical regions relates to the composition of their connected callosal fibers, we conducted the analyses discussed above. We quantified cortical myelin content by adopting the HCP group-averaged T1w/T2w values on the standard 32k_fs_LR surface (https://balsa.wustl.edu/file/show/zpL2m)[55]. Similarly, we quantified callosal fiber composition by adopting the HCP group-averaged values of two dMRI-derived parameters on the template mCC: neurite density index (NDI) and orientation dispersion index (ODI)[33]. For each pair of homotopic regions from the 4 cortical parcellations above (i.e., BNA, HCPMMP, Schaefer_L/Schaefer_R), the regional mean T1w/T2w ratio value was calculated and then averaged between the left and right regions; for the passing mCC region of each homotopic region pair (derived from the thresholded mCC topographic map at $p = 0.05$), the mean NDI and ODI values were calculated. For each cortical parcellation, Pearson correlation between the T1/T2 ratio and NDI or ODI values was then evaluated across all cortical regional pairs.

References

1. Gazzaniga, M. S. Cerebral specialization and interhemispheric communicationDoes the corpus callosum enable the human condition? *Brain* **123**, 1293–1326 (2000).
2. Shen, K. *et al.* Stable long-range interhemispheric coordination is supported by direct anatomical projections. *Proc. Natl. Acad. Sci.* **112**, 6473–6478 (2015).
3. Suárez, R. *et al.* A pan-mammalian map of interhemispheric brain connections predates the evolution of the corpus callosum. *Proc. Natl. Acad. Sci.* **115**, 9622–9627 (2018).
4. Roland, J. L. *et al.* On the role of the corpus callosum in interhemispheric functional connectivity in humans. *Proc. Natl. Acad. Sci.* **114**, 13278–13283 (2017).
5. Innocenti, G. M. *et al.* The functional characterization of callosal connections. *Prog. Neurobiol.* **208**, 102186 (2022).
6. Josse, G., Seghier, M. L., Kherif, F. & Price, C. J. Explaining Function with Anatomy: Language Lateralization and Corpus Callosum Size. *J. Neurosci.* **28**, 14132–14139 (2008).
7. Luders, E. *et al.* The link between callosal thickness and intelligence in healthy children and adolescents. *NeuroImage* **54**, 1823–1830 (2011).
8. Wolff, J. J. *et al.* Altered corpus callosum morphology associated with autism over the first 2 years of life. *Brain J. Neurol.* **138**, 2046–2058 (2015).
9. Fan, Q. *et al.* Age-related alterations in axonal microstructure in the corpus callosum measured by high-gradient diffusion MRI. *NeuroImage* **191**, 325–336 (2019).
10. Sunderland, S. THE DISTRIBUTION OF COMMISSURAL FIBRES IN THE CORPUS CALLOSUM IN THE MACAQUE MONKEY. *J. Neurol. Psychiatry* **3**, 9–18 (1940).
11. Pandya, D. N., Karol, E. A. & Heilbronn, D. The topographical distribution of interhemispheric projections in the corpus callosum of the rhesus monkey. *Brain Res.* **32**, 31–43 (1971).
12. Swadlow, H. A., Rosene, D. L. & Waxman, S. G. Characteristics of interhemispheric impulse conduction between prelunate gyri of the rhesus monkey. *Exp. Brain Res.* **33**, 455–467 (1978).
13. Barbas, H. & Pandya, D. N. Topography of commissural fibers of the prefrontal cortex in the rhesus monkey. *Exp. Brain Res.* **55**, 187–191 (1984).
14. Cipolloni, P. B. & Pandya, D. N. Topography and trajectories of commissural fibers of the superior temporal region in the rhesus monkey. *Exp. Brain Res.* **57**, 381–389 (1985).
15. Rockland, K. S. & Pandya, D. N. Topography of occipital lobe commissural connections in the rhesus monkey. *Brain Res.* **365**, 174–178 (1986).
16. Caminiti, R., Ghaziri, H., Galuske, R., Hof, P. R. & Innocenti, G. M. Evolution amplified processing with temporally dispersed slow neuronal connectivity in primates. *Proc. Natl. Acad. Sci. U. S. A.* **106**, 19551–19556 (2009).
17. de Lacoste, M. C., Kirkpatrick, J. B. & Ross, E. D. Topography of the Human Corpus Callosum. *J. Neuropathol. Exp. Neurol.* **44**, 578–591 (1985).

18. Huang, H. *et al.* DTI tractography based parcellation of white matter: Application to the mid-sagittal morphology of corpus callosum. *NeuroImage* **26**, 195–205 (2005).
19. Hofer, S. & Frahm, J. Topography of the human corpus callosum revisited—Comprehensive fiber tractography using diffusion tensor magnetic resonance imaging. *NeuroImage* **32**, 989–994 (2006).
20. Zarei, M. *et al.* Functional anatomy of interhemispheric cortical connections in the human brain. *J. Anat.* **209**, 311–320 (2006).
21. Witelson, S. F. Hand and sex differences in the isthmus and genu of the human corpus callosum. A postmortem morphological study. *Brain J. Neurol.* **112 (Pt 3)**, 799–835 (1989).
22. Park, H.-J. *et al.* Corpus callosal connection mapping using cortical gray matter parcellation and DT-MRI. *Hum. Brain Mapp.* **29**, 503–516 (2008).
23. Chao, Y.-P. *et al.* Probabilistic topography of human corpus callosum using cytoarchitectural parcellation and high angular resolution diffusion imaging tractography. *Hum. Brain Mapp.* **30**, 3172–3187 (2009).
24. Pannek, K. *et al.* An automated strategy for the delineation and parcellation of commissural pathways suitable for clinical populations utilising high angular resolution diffusion imaging tractography. *NeuroImage* **50**, 1044–1053 (2010).
25. Dougherty, R. F., Ben-Shachar, M., Bammer, R., Brewer, A. A. & Wandell, B. A. Functional organization of human occipital-callosal fiber tracts. *Proc. Natl. Acad. Sci. U. S. A.* **102**, 7350–7355 (2005).
26. Wahl, M. *et al.* Human Motor Corpus Callosum: Topography, Somatotopy, and Link between Microstructure and Function. *J. Neurosci.* **27**, 12132–12138 (2007).
27. Saenz, M. & Fine, I. Topographic organization of V1 projections through the corpus callosum in humans. *NeuroImage* **52**, 1224–1229 (2010).
28. Van Essen, D. C. *et al.* The WU-Minn Human Connectome Project: an overview. *NeuroImage* **80**, 62–79 (2013).
29. Aboitiz, F., Scheibel, A. B., Fisher, R. S. & Zaidel, E. Fiber Composition of the Human Corpus-Callosum. *Brain Res.* **598**, 143–153 (1992).
30. Fan, L. *et al.* The Human Brainnetome Atlas: A New Brain Atlas Based on Connectional Architecture. *Cereb. Cortex* **26**, 3508–3526 (2016).
31. Glasser, M. F. *et al.* A multi-modal parcellation of human cerebral cortex. *Nature* **536**, 171–178 (2016).
32. Schaefer, A. *et al.* Local-Global Parcellation of the Human Cerebral Cortex from Intrinsic Functional Connectivity MRI. *Cereb. Cortex* **28**, 3095–3114 (2018).
33. Zhang, H., Schneider, T., Wheeler-Kingshott, C. A. & Alexander, D. C. NODDI: Practical in vivo neurite orientation dispersion and density imaging of the human brain. *NeuroImage* **61**, 1000–1016 (2012).
34. Rosas, H. D. *et al.* Altered white matter microstructure in the corpus callosum in Huntington's disease: Implications for cortical "disconnection". *NeuroImage* **49**, 2995–3004 (2010).
35. Li, J. *et al.* A comparative diffusion tensor imaging study of corpus callosum subregion integrity in bipolar disorder and schizophrenia. *Psychiatry Res. Neuroimaging* **221**, 58–62 (2014).

36. Bledsoe, I. O., Stebbins, G. T., Merkitch, D. & Goldman, J. G. White matter abnormalities in the corpus callosum with cognitive impairment in Parkinson disease. *Neurology* **91**, e2244–e2255 (2018).
37. Tournier, J.-D., Calamante, F. & Connelly, A. Robust determination of the fibre orientation distribution in diffusion MRI: non-negativity constrained super-resolved spherical deconvolution. *NeuroImage* **35**, 1459–1472 (2007).
38. Smith, R. E., Tournier, J. D., Calamante, F. & Connelly, A. Anatomically-constrained tractography: improved diffusion MRI streamlines tractography through effective use of anatomical information. *NeuroImage* **62**, 1924–38 (2012).
39. Smith, R. E., Tournier, J. D., Calamante, F. & Connelly, A. SIFT: Spherical-deconvolution informed filtering of tractograms. *NeuroImage* **67**, 298–312 (2013).
40. Friston, K. J. *et al.* Statistical parametric maps in functional imaging: A general linear approach. *Hum. Brain Mapp.* **2**, 189–210 (1994).
41. Smith, S. M. & Nichols, T. E. Threshold-free cluster enhancement: Addressing problems of smoothing, threshold dependence and localisation in cluster inference. *NeuroImage* **44**, 83–98 (2009).
42. Woo, C.-W., Krishnan, A. & Wager, T. D. Cluster-extent based thresholding in fMRI analyses: Pitfalls and recommendations. *NeuroImage* **91**, 412–419 (2014).
43. Vos de Wael, R. *et al.* BrainSpace: a toolbox for the analysis of macroscale gradients in neuroimaging and connectomics datasets. *Commun. Biol.* **3**, 1–10 (2020).
44. Zhou, J. *et al.* Axon position within the corpus callosum determines contralateral cortical projection. *Proc. Natl. Acad. Sci.* **110**, E2714–E2723 (2013).
45. Chklovskii, D. B., Schikorski, T. & Stevens, C. F. Wiring Optimization in Cortical Circuits. *Neuron* **34**, 341–347 (2002).
46. Bullmore, E. & Sporns, O. The economy of brain network organization. *Nat. Rev. Neurosci.* **13**, 336–349 (2012).
47. Tovar-Moll, F. *et al.* Structural and functional brain rewiring clarifies preserved interhemispheric transfer in humans born without the corpus callosum. *Proc. Natl. Acad. Sci.* **111**, 7843–7848 (2014).
48. Wedeen, V. J. *et al.* The Geometric Structure of the Brain Fiber Pathways. *Science* **335**, 1628–1634 (2012).
49. Yang, L. *et al.* Callosal fiber length scales with brain size according to functional lateralization, evolution, and development. *J. Neurosci.* (2022) doi:10.1523/JNEUROSCI.1510-21.2022.
50. Glasser, M. F. *et al.* The minimal preprocessing pipelines for the Human Connectome Project. *NeuroImage* **80**, 105–124 (2013).
51. Jeurissen, B., Tournier, J.-D., Dhollander, T., Connelly, A. & Sijbers, J. Multi-tissue constrained spherical deconvolution for improved analysis of multi-shell diffusion MRI data. *NeuroImage* **103**, 411–426 (2014).
52. Tournier, J.-D. *et al.* MRtrix3: A fast, flexible and open software framework for medical image processing and visualisation. *NeuroImage* **202**, 116137 (2019).
53. Smith, S. M. *et al.* Advances in functional and structural MR image analysis and implementation as FSL. *NeuroImage* **23**, S208–S219 (2004).
54. Sherif, T., Kassis, N., Rousseau, M.-É., Adalat, R. & Evans, A. C. BrainBrowser:

distributed, web-based neurological data visualization. *Front. Neuroinformatics* **8**, 89 (2015).
55. Glasser, M. F. *et al.* Empirical transmit field bias correction of T1w/T2w myelin maps. *NeuroImage* **258**, 119360 (2022).

Acknowledgments

This work was supported by the Science and Technology Innovation 2030-Brain Science and Brain-Inspired Intelligence Project of China (grant no. 2021ZD0201701, 2021ZD0200502, G.G.) and National Science Foundation of China (82172016, G.G.). Data were provided by the Human Connectome Project, WU-Minn Consortium (Principal Investigators: David Van Essen and Kamil Ugurbil; 1U54MH091657) funded by the 16 NIH Institutes and Centers that support the NIH Blueprint for Neuroscience Research; and by the McDonnell Center for Systems Neuroscience at Washington University.

Author contributions

G.G. designed and coordinated the research. Y.X. performed the research. Y.X., L.Y., C.W., C.Z., J.L., and D.W. analyzed the data. Y.X., C.W., and Y.O. developed the online tool. Y.X., M.T.d.S., and G.G. wrote the manuscript, which was edited by all authors.

Conflict of interests

The authors declare no competing financial interests.

Table 1. Comparison of existing histological monkey or human mapping results of callosal connections with our currently estimated population-based topographic results.

Literature	Species	Trace injection site	Reported connectional position	Consistency with our results
Sunderland (1940)	Macaca	frontal	the genu and anterior third of the body	√
		occipital	splenium and posterior third of the body (isthmus)	√
		parietal and temporal	posterior two-thirds of the body (isthmus)	√
Pandya et al. (1971)	Macaca mulatta	rostral half	frontal lobe	√
		caudal half	parietal, temporal and occipital lobe and insulo-opercular region	√
		splenium	occipital lobe and prostriate area	√
		midline in the posterior half	precentral opercula	√
		caudal part of the body	temporal lobe	√
Swadlow et al. (1978)	Macaca mulatta	prelunate gyri	splenium	√
Barbas and Pandya (1984)	Macaca mulatta	area 46	genu and anterior body	√
		area 25 and 32	genu	√
		area 13 and 14	anterior portion of the genu, and the rostrum	√
		area 8	the border of the genu and the body	√
		area 46v and area 12	genu	√
Cipolloni and Pandya (1985)	Macaca mulatta	paAlt and Ts3	rostral to splenium	√
Rockland and Pandya (1986)	Macaca mulatta	area 18	posterior 3-4 mm of the splenium	√
		area 19	splenium, dorsal to area 18	√
Caminiti et al. (2009)	Macaca fascicularis	area 9 and 9/46 border	genu	√
		area 6 and F4	anterior part of body	√
		area 4	posterior part of body	√
		area 2	isthmus	√
		area 5	posterior part of isthmus and splenium	√
		areas 17 and 18	posterior part of splenium	√
de Lacoste et al. (1985)	Human	inferior frontal and anterior inferior parietal	genu	√
		posterior superior frontal	body	√
		temporo-parieto-occipital junction	splenium	√

	superior parietal region	splenium	√
	occipital lobe region	splenium	√
	mid-temporal region	Anterior body	×

Note: For detailed topographic maps, please see Fig. S3: 1-8.

Figures

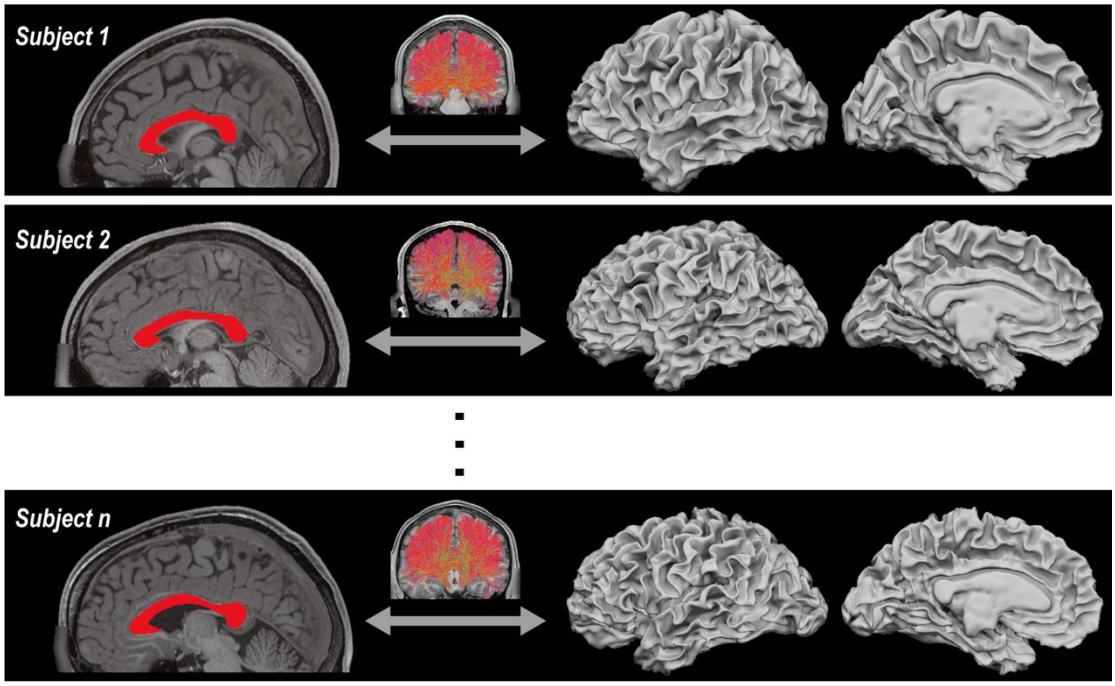

Figure 1. Schematics of estimating individual-level callosal connections between the mCC and cortical regions on the white surface via diffusion MRI-based fiber tracking. For selected individuals, the mCC mask (left), callosal fibers (middle), and cortical white surface (right) were displayed.

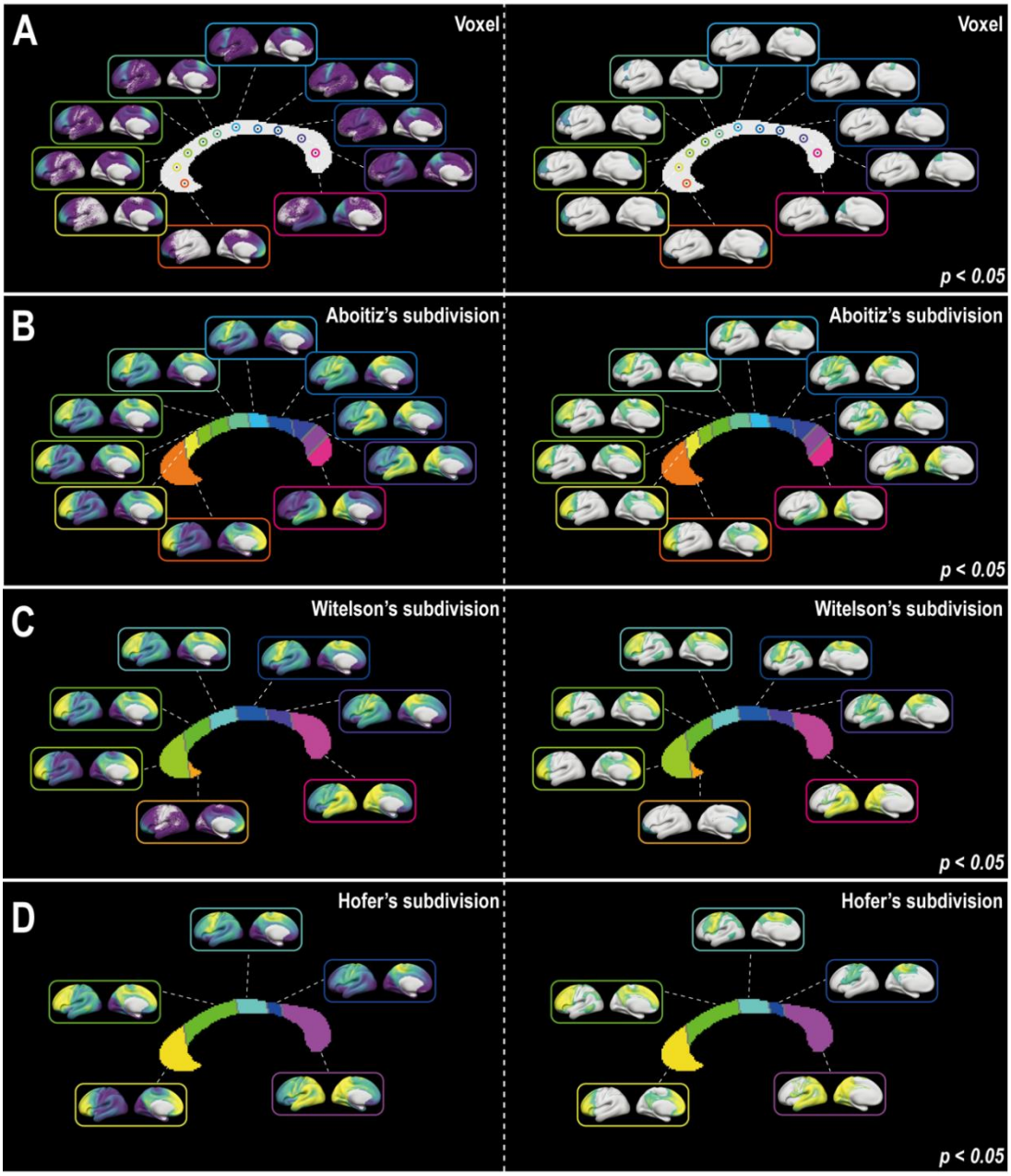

Figure 2. Population-based probability-weighted cortical topographies for mCC voxels and subdivisions. (A) Cortical topographic maps for 10 selected voxels on the mCC. Each voxel is indicated by a small circle. (B) Cortical topographic maps for the 10 mCC subdivisions from the Aboitiz parcellation[29]. (C) Cortical topographic maps for the 7 mCC subdivisions from the Witelson parcellation[21]. (D) Cortical topographic maps for the 5 mCC subdivisions from the Hofer parcellation[19]. The nonthresholded and thresholded (i.e., $p < 0.05$) maps are illustrated in the left and right panels, respectively.

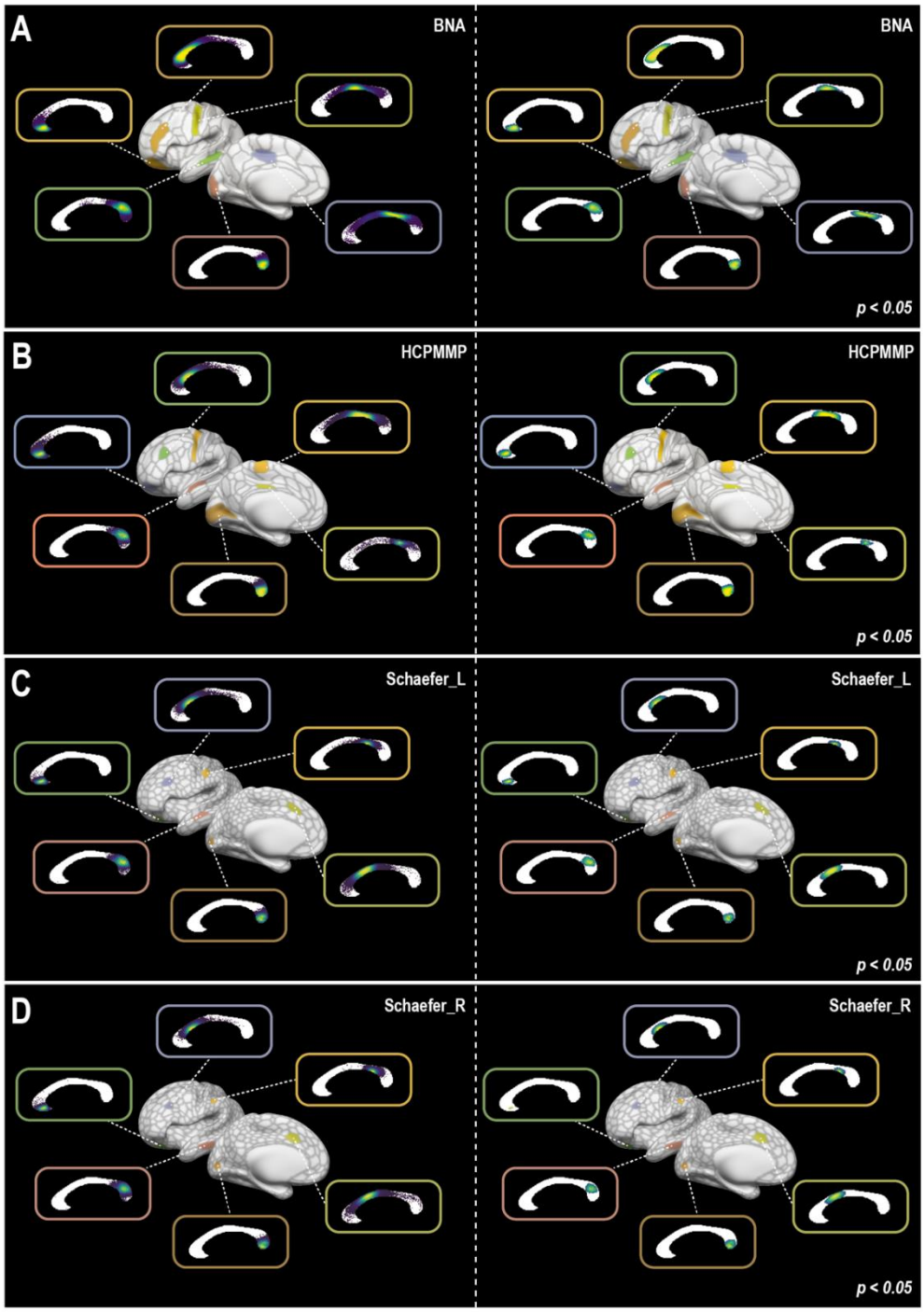

Figure 3. Population-based probability-weighted mCC topographies for homotopic cortical regional pairs. (A) mCC topographic maps for 6 selected homotopic cortical regional pairs from the BNA[30]. The selected regions are indicated by specific colors on the cortical surface. (B) mCC topographic maps for 6 selected homotopic cortical regional pairs from the HCPMMP[31]. The selected regions are indicated by specific colors on the cortical surface. (C) mCC topographic maps for 6 selected homotopic cortical regional pairs from the Schaefer_L parcellation[32]. (D) mCC topographic maps for 6 selected homotopic cortical regional pairs from the Schaefer_R parcellation[32]. The nonthresholded and thresholded (i.e., $p < 0.05$) maps are illustrated in the left and right panels, respectively.

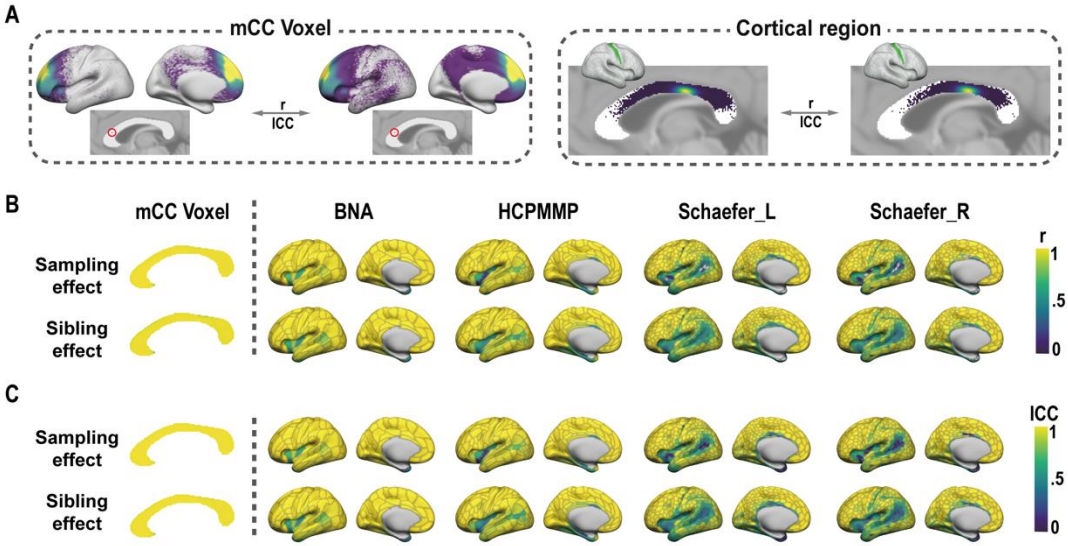

Figure 4. Reproducibility of probability-weighted topographic maps: the sampling and sibling effects. (A) The schematics of measuring spatial similarity between two topographic maps. Left: measuring similarity between two cortical topographic maps for each mCC voxel. One example voxel (red circle) is selected, and its cortical topographic map is displayed. Right: measuring similarity between two mCC topographic maps for each pair of homotopic regions. One example cortical region (green) is selected, and its mCC topographic map is displayed. R: Pearson correlation; ICC: intraclass correlation. **(B)** The r-based similarity of topographic maps between two split-half HCP samples (i.e., the sampling effect, top row) and between unrelated and whole HCP samples (i.e., the sibling effect, bottom row). **(C)** The ICC-based similarity of topographic maps between two split-half HCP samples (i.e., the sampling effect, top row) and between unrelated and whole HCP samples (i.e., the sibling effect, bottom row). The relevant results for relative streamline number-weighted topographic maps are included in Figure S3.

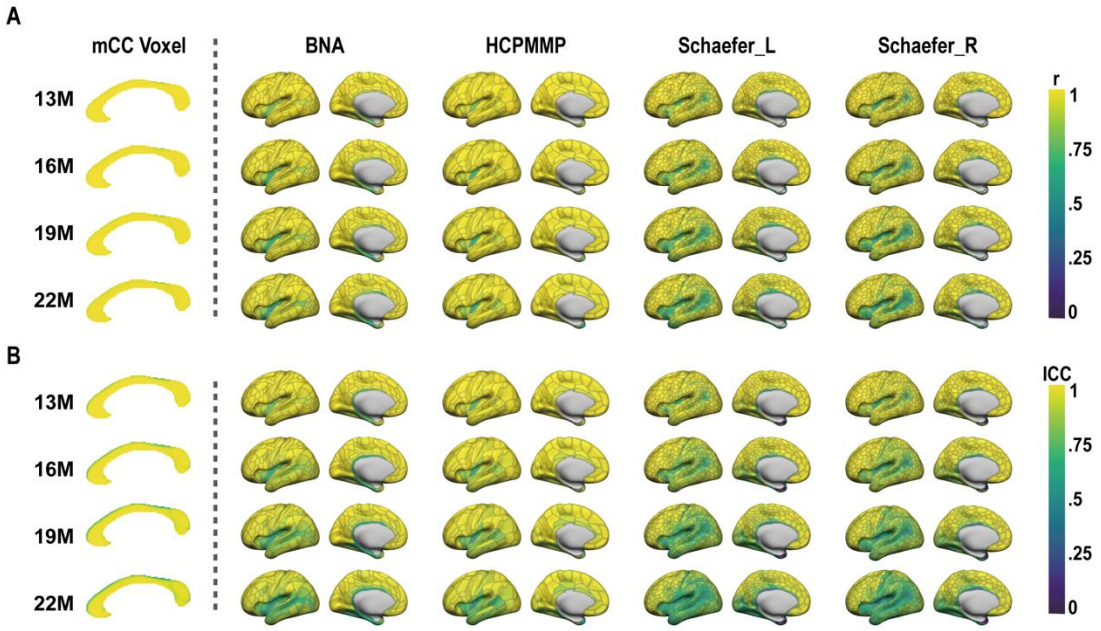

Figure 5. Reproducibility of probability-weighted topographic maps: the effect of initially generated streamline number. (A) The r-based similarity of topographic maps between our main results from 10 M initially generated streamlines and others from more streamlines (i.e., 13 M, 16 M, 19 M, 22 M). **(B)** The ICC-based similarity of topographic maps between our main results from 10 M initially generated streamlines and others from more streamlines (i.e., 13 M, 16 M, 19 M, 22 M). The relevant results for relative streamline number-weighted topographic maps are included in Figure S4.

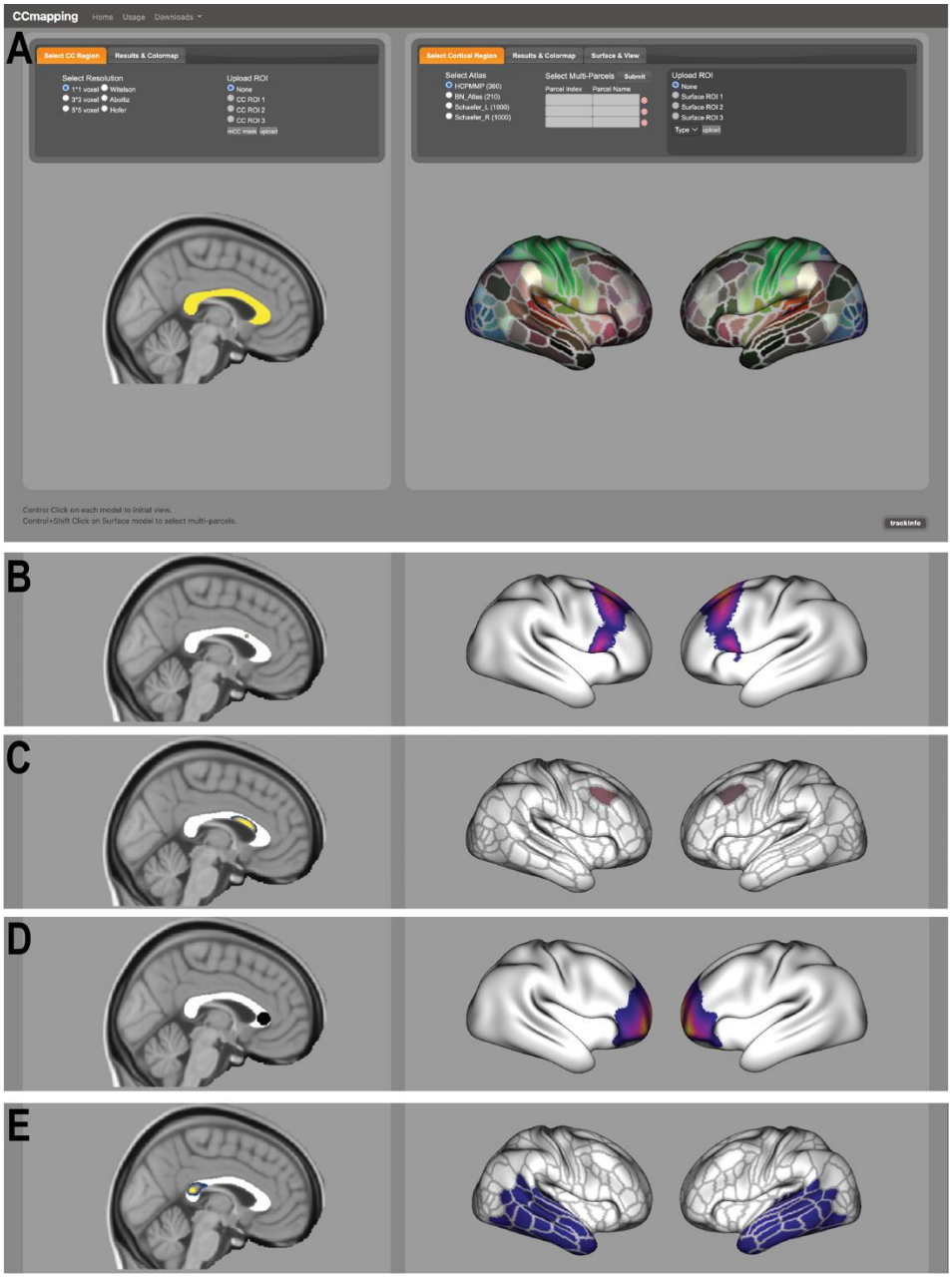

Figure 6. *CCmapping* for visualizing cortical or mCC topographic maps. (A) The interface of *CCmapping*. (B) Snapshot visualizing the cortical topographic map for an example selected voxel on the mCC. (C) Snapshot visualizing the mCC topographic map for an example selected cortical region. (D) Snapshot visualizing the cortical topographic map for an example customized ROI on the mCC. (E) Snapshot visualizing the mCC topographic map for an example customized cortical ROI.

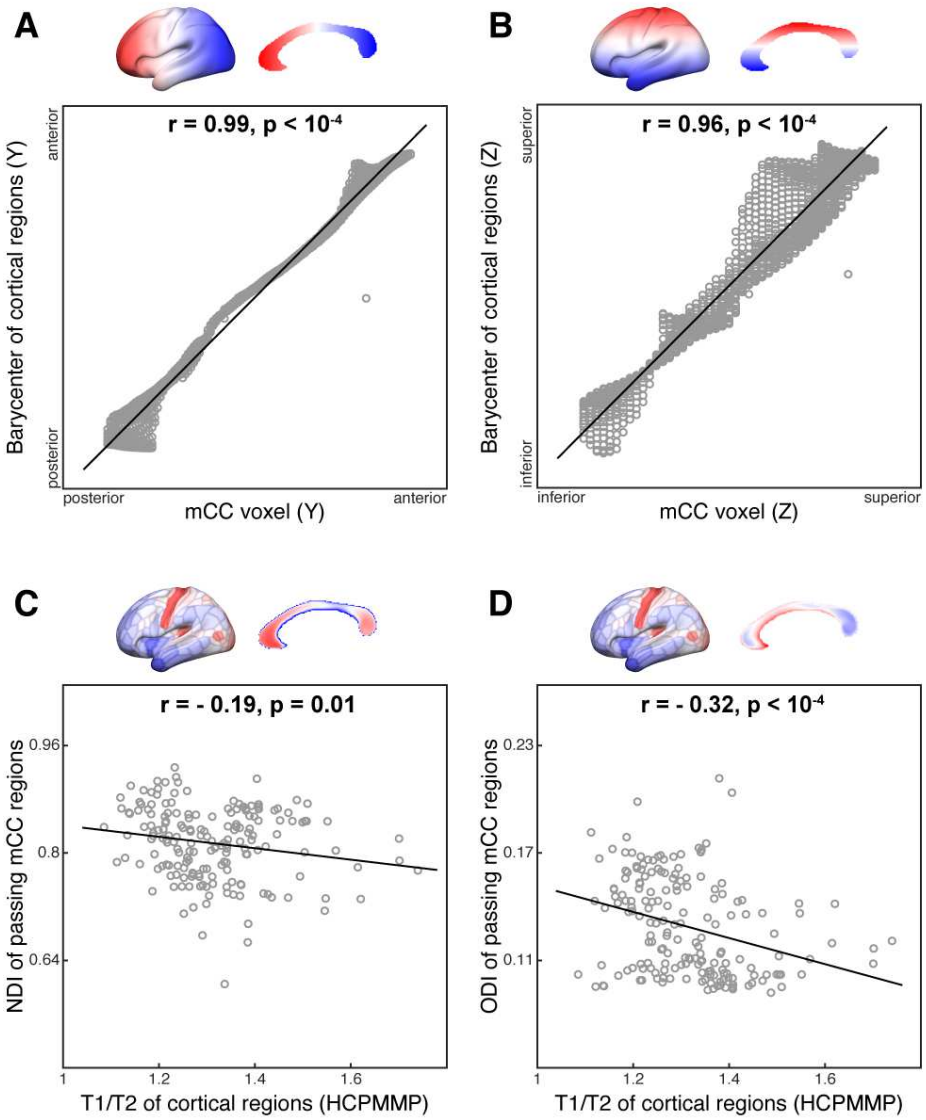

Figure 7. Assessing relationships between callosal fibers and their connected cortical regions by population-based topographic maps. (A) The correlation of the Y and Z coordinates of mCC voxels with the barycenter of their connected cortical regions. The connected cortical region for each mCC voxel was derived from the thresholded mCC topographic map at p = 0.05. The Y and Z coordinates represent the relative positioning along the anterior-posterior (A-P) and dorsal-ventral (D-V) axes, respectively. (B) The correlation of the T1/T2 ratio values of cortical regions with the NDI and ODI values of their passing mCC region. The passing mCC region for each homotopic region pair was derived from the thresholded mCC topographic map at p = 0.05.

Supplementary Files

This is a list of supplementary files associated with this preprint. Click to download.

- ManuscriptSMfinal.pdf